LETTER

All-optical polarization tuning based on an intensity-dependent nonlinear metasurface

Letters

IOP Publishing

Journal of Physics D: Applied Physics

J. Phys. D: Appl. Phys. **56** (2023) 15LT01 (6pp)

https://doi.org/10.1088/1361-6463/acbce1

Letter

All-optical polarization tuning based on an intensity-dependent nonlinear metasurface

Yaping Hou[1], Jianyong Mao[1], Tianlun Li[1], Yunfan Xu[1], Weitao Jiang[2], Yanpeng Zhang[1] and Lei Zhang[1,*]

[1] Key Laboratory of Physical Electronics and Devices of Ministry of Education & Shaanxi Key Laboratory of Information Photonic Technique, School of Electronic Science and Engineering, Xi'an Jiaotong University, Xi'an 710049, People's Republic of China

[2] State Key Laboratory for Manufacturing Systems Engineering, Xi'an Jiaotong University, Xi'an 710049, People's Republic of China

E-mail: eiezhanglei@xjtu.edu.cn

Received 22 November 2022, revised 1 February 2023
Accepted for publication 17 February 2023
Published 13 March 2023

Abstract

Active control of light polarization at the nanoscale is essential for integrated photonic devices. Here, an all-optical approach is proposed to tune the polarization state of near-infrared light using a nonlinear metasurface. Based on the large intensity-dependent refractive index change of epsilon-near-zero (ENZ) materials, a phase difference between two orthogonal electric fields at ENZ wavelength can be continuously tuned in a range larger than 0.61π by varying the incident light power. The polarization state of the reflected light can thus be actively tuned from linear to circular state via an all-optical approach. Notably, abundant polarization states can be obtained by altering the polarization angle of incident light. The proposed all-optical approach is promising for tunable photonic functionalities of practical applications.

Keywords: polarization modulator, intensity-dependent refractive index, epsilon-near-zero

(Some figures may appear in colour only in the online journal)

Polarization, as one of the fundamental properties of light, is highly involved in practical photonics applications [1]. Conventional retarders and polarizers can change the light polarization by controlling the phase difference and amplitude ratio of two orthogonal electric field components. However, current commercial elements possess bulk features, which make it difficult to apply in highly integrated photonic devices. As the development of nanofabrication technologies, the footprint of the optical element approaches nanometer scale, while new challenges arise with the efficient and flexible control over polarization states. It becomes important to realize dynamic polarization control elements with nanoscale structures for multifunctional devices [2, 3]. Subsequently, various methods are proposed to achieve active polarization manipulation, such as mechanical deformation, thermo-induced phase change and electrical tuning [4–6]. In contrast, all-optical approaches have high modulation speed at the terahertz level and low energy consumption [7–9]. Lately, typical epsilon-near-zero (ENZ) materials, such as indium tin oxide (ITO) and indium-doped cadmium oxide, were utilized to achieve a dynamic polarization rotation. However, the maximum phase change was very

* Author to whom any correspondence should be addressed.

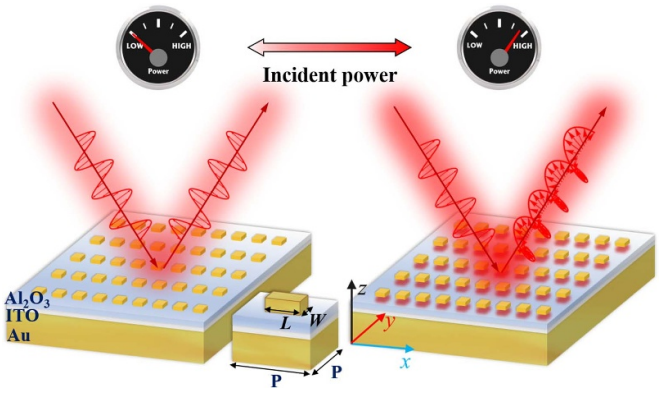

Figure 1. Schematic of the nonlinear metasurface for all-optical polarization tuning.

limited and the polarization was merely switched from linear polarization to elliptical polarization [10, 11].

The refractive index modulation based on optical Kerr effect can be used for polarization switching by controlling the incident power level. However, the refractive index change of traditional nonlinear optical materials is extremely weak even under strong laser irradiation, which precludes the applications from active retarders and polarizers with small footprint [12]. Recently, ITO, as an ENZ material, has emerged as an appealing alternative with large optical nonlinear processes [13–15] including harmonic generation [16] and refractive index modulation [17]. A large intensity-dependent refractive index change provides a superior platform for reversible and ultrafast all-optical nanophotonic devices.

Here, a nonlinear metasurface based on intensity-dependent refractive index change is proposed to actively tune the polarization state of the reflected light at near infrared (NIR) frequency. By employing the gap mode with enhanced local electric field, a near unity refractive index variation is achieved to provide a large phase modulation range by varying the power of incident light. As the light intensity increases, the polarization state of the reflected light can be continuously tuned from the linear to the elliptical polarization state, and then to the circular polarization state. We believe that the proposed all-optical approach can offer a feasible platform to realize tunable and miniaturized optical elements.

Figure 1 shows the schematic of the proposed nonlinear metasurface, which consists of typical metal/insulator/metal (MIM) configurations (figure 1). The bottom gold layer is used to block the transmission. Gold nanobricks on the top of aluminum oxide (Al_2O_3)/ITO layer provide the anisotropic electromagnetic responses for polarization control. The MIM structure supports a typical gap mode with electric field being strongly confined at the insulator layer. It is initially being proposed as a perfect absorber [18, 19]. Similar structures have been widely used to control the amplitude, phase and polarization of reflected light. Later, it was extended for more functions, such as anonymous beam reflection [20] and hologram [21]. Furthermore, it can be leveraged to generate various polarization states covering a broad band [22]. It is well known that the localized resonant properties are highly sensitive to the change in immediate dielectric environment. ITO layer is capable of providing the required refractive index change to induce a considerable phase and amplitude variation. Due to the isotropic properties of the ITO film, the designed polarization switching relies on the artificial anisotropy of the top nanostructures (figure 1). When rectangular nanobricks are chosen with an optimized size, the phase and amplitude will evolve independently and the polarization can then be manipulated by means of the intensity-dependent refractive index caused beneath the top nanostructures.

The insulator part consists of thin layers of Al_2O_3 and ITO. The ITO layer gives rise to the polarization tunability of entire design via the refractive index change, while the Al_2O_3 layer is inserted as an additional freedom for phase tuning. The refractive index change arising from optical Kerr effect is $\Delta n = n_2 I$, where n_2 is the nonlinear refractive index and I is the electric field intensity. Under the perturbation theory, the nonlinear refractive index can be expressed as

$$n_2 = \frac{3\chi^{(3)}}{4n_0^2\varepsilon_0 c}, \tag{1}$$

where $\chi^{(3)}$ is the third-order susceptibility [12]. In principle, a magnified nonlinear refractive index can be obtained if the real part of linear refractive index n_0 is smaller than one. Thus, a giant refractive index change could be obtained even larger than the linear counterpart. Fortunately, such an enhancement can occur at the adjacent range of its ENZ wavelength λ_{ENZ}, with a bandwidth of ~80 nm, where the real part of refractive index is smaller than one (figure 2(a) blue area) [17]. The underlying mechanism can be understood that when a pumping light at ENZ wavelength is incident, the free carriers experience intraband transitions in the ENZ material, which increase the effective mass of carriers. Therefore, the plasma frequency decreases and induces a change in permittivity of ENZ material. Currently, the nonlinear refractive index of ITO is only extensively investigated at the λ_{ENZ} of 1240 nm [23]. For this reason, the all-optical polarization tuning is performed only at the ENZ wavelength. Interestingly, the significant refractive index change can be potentially enhanced within a broad wavelength band [24]. Nevertheless, it should be noted that the above expression of nonlinear refractive index of equation (1) becomes invalid when n_2 is too large. Instead, the original definition of refractive index should be resorted for refractive index calculation, i.e., $n_{NL}(\boldsymbol{r},\omega) = \sqrt{\varepsilon_{NL}(\boldsymbol{r},\omega)}$. The nonlinear permittivity $\varepsilon_{NL}(\boldsymbol{r},\omega)$ can be written as

$$\varepsilon_{NL}(\boldsymbol{r},\omega) \approx \varepsilon_L + \sum_{j=1}^{3} c_{2j+1}\chi^{2j+1}(\omega)\left|\frac{\boldsymbol{E}(\boldsymbol{r},\omega)}{2}\right|^{2j}, \tag{2}$$

where χ^{2j+1} is the $(2j+1)$-order nonlinear susceptibilities; $c_3 = 3$, $c_5 = 10$ and $c_7 = 35$ are the degeneracy factors [23, 25]. The electric field $\boldsymbol{E}(\boldsymbol{r},\omega)$ indicates that the optically induced refractive index change is dependent not only on the amplitude but also on the spatial distribution of electric field inside the

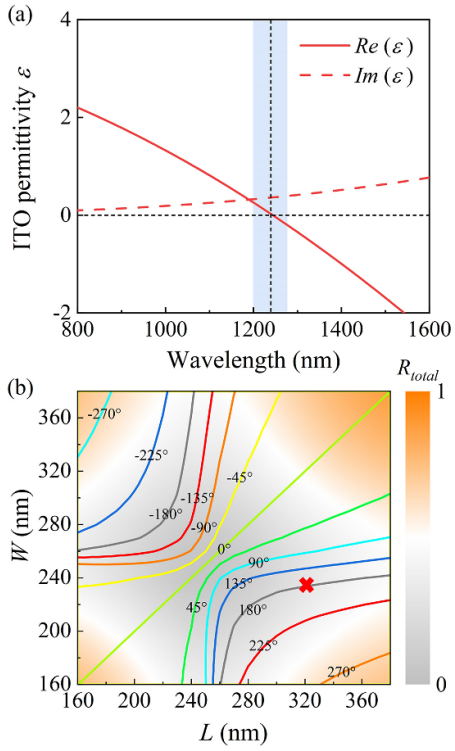

Figure 2. (a) Permittivity of ITO layer. The blue area indicates the ENZ region, in which the wavelength range with a real part of linear refractive index n_0 being smaller than 1. (b) Dependence of total reflectance (R_{total}) and phase difference (colorful contour lines) at the ENZ wavelength by varying the size of the top nanostructure. The incident light is linearly polarized with a polarization angle of 45° with respect to x-axis. The red cross indicates the selected nanobrick dimensions $L \times W = 325$ nm $\times$ 235 nm for an exemplary demonstration of polarization tuning.

nonlinear medium. Notably, the intensity-dependent nonlinear refractive index of ITO was calculated using Stationary Solver in COMSOL software. According to equation (2), the spatial electric field results in an associated variation to the refractive index inside ITO layer. After several iterations, the distributions of both the electric field and refractive index become converged.

An input light beam with arbitrary polarization state can be decomposed into two orthogonal components along the x- and y-axes. The final polarization state of the output signal is thus dependent on the phase difference and amplitude ratio of the two field components. Due to the anisotropic nature of the metasurface used in this work, the complex reflection coefficients of two orthogonal parts differs from each other. As the incident power increases, the reflection coefficients of two orthogonal polarizations varies independently. Consequently, the polarization state of reflected light can be dynamically tuned in an all-optical way in comparison with the static output signal. Notably, when a localized resonant mode is excited, the refractive index of ITO layer varies spatially due to the intensity-dependent nonlinear effect.

To efficiently tune the polarization state, it is highly necessary to investigate the dependence of reflection and phase change on the geometry size. All the simulations are performed using commercial software COMSOL Multiphysics based on the finite element method. The dielectric constant of gold is extracted from experimental data [26] and the refractive index of Al_2O_3 is set to be 1.751. Perfectly matched layer boundary conditions are applied along z-axis, while Floquet periodic boundary conditions are applied along x- and y-axes. The top nanostructures are arranged in a square lattice with a period P of 400 nm, which is much smaller than the operation wavelength. Therefore, no diffraction effect occurs in the following calculations. A plane wave with a linear polarization is normally incident on the proposed structure and the polarization state of reflected light is acquired by analyzing the phase difference and amplitude ratio of electric field. After some preliminary optimizations, the thicknesses of the top Au nanobricks and Al_2O_3 layer are set to be 30 nm and 40 nm, respectively, while the thickness of ITO is set to be 20 nm, which is thinner than skin depth of ITO [27]. Since the planar films and substrate are isotropic, the polarization state is finally determined by the anisotropic response of the top structures. Therefore, the geometry-dependent reflectance and phase delay are synthetically investigated by sweeping the length and width of the top gold nanobricks.

In linear optical case, a 45°-polarized plane wave is normally incident on the structure along z-axis. The phase δ_x (δ_y) and amplitude of E_x (E_y) component are extracted from the reflected electric field (figure 2(a)). The amplitude ratio and the phase difference δ ($= \delta_y - \delta_x$) between the E_y and E_x components have complex relationship with the geometry size (figure 2(b)). In the survey scope, the phase difference covers a range even larger than 3π, which is potentially competent for flexible polarization tuning. Although the phase difference and amplitude of localized mode is sensitive to the refractive index change, it is still necessary to select a candidate structure locating at the range with a large phase gradient as the geometry varies (figure 2(b)). It is found that such type of structures usually supports a small reflectance, which indicates a low manipulation efficiency. After carefully exploring the geometry dependence, the structure with $L = 325$ nm and $W = 235$ nm is selected, which supports a phase difference of π. However, the proposed structure possesses several geometry parameters, which make the optimization process even more challenging. Therefore, other advanced optimization techniques, such as deep learning, may be employed to further optimize the geometry size for both high reflectance and large phase variation [28, 29].

The refractive index change caused by nonlinear effect is dependent on the light intensity. Then the phase and amplitude response of the reflected light is investigated by increasing the incident intensity (figure 3). As the incident power increases, the resonant spectrum redshifts due to the increase in refractive index. The reflected electric field amplitudes of both orthogonal components increase with a comparable rate (figure 3(a)). Therefore, the amplitude ratio of two components maintains around 1 (figure 3(b)). In contrast, the phase delay δ_x of E_x decreases slightly, while the phase delay δ_y of E_y decreases rapidly (figure 3(a)). It is obvious that the resonance along y-axis mainly contributes to the decrease of phase difference δ between two components (figure 3(b)). When a

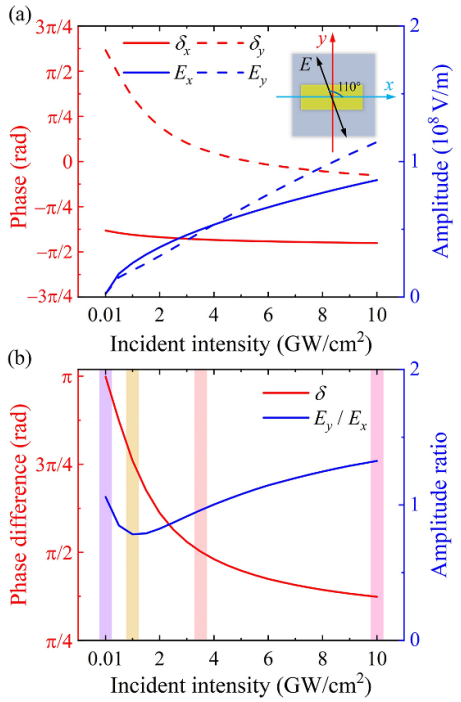

Figure 3. (a) Dependence of phase and electric field amplitude of the reflected x- and y-component on the incident intensity. (b) Dependence of phase difference and amplitude ratio of two orthogonal components on the incident intensity. Here, light is normally incident; structure size $L = 325$ nm and $W = 235$ nm.

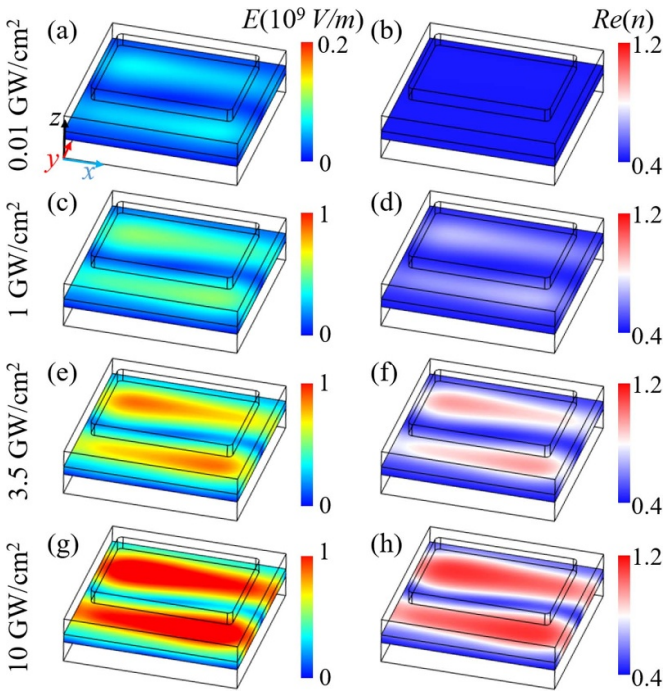

Figure 4. Correlation between electric field distribution (left column) and refractive index inside at the ITO layer (right column) as the incident intensity increases. Here, structure size $L = 325$ nm and $W = 235$ nm.

low intensity is 0.01 GW cm^{-2} is incident, the refractive index change is negligible and the phase difference is π, i.e. linear optical case. As the incident intensity gradually increases to 10 GW cm^{-2}, the phase difference becomes even smaller than 0.5π which should be attributed to the optically induced refractive index change. Remarkably, the range of phase difference δ change is larger than 0.5π, which outperforms most of the existing works based on all-optical tuning scheme. Moreover, it is found that both phase difference and amplitude ratio gradually reach a plateau as the intensity increases, which may result from the deviating from the resonance in case of large index change. Such a scenario is beneficial for achieving a quarter waveplate using a moderate incident intensity.

The correlation between electric field and refractive index change is further analyzed (figure 4). The refractive index change caused by the intensity-dependent nonlinear effect holds similar spatial distribution to the local electric field (figure 4). For example, under the illumination of 110°-polarized light, the resonance along y-axis dominates the field distribution (figure 4), which gives rise to the fast phase change of δ_y of E_y component (figure 3(a)). When the incident intensity is as low as 0.01 GW cm^{-2}, the field distribution is almost symmetric along y-axis (figure 4(a)). However, since the field intensity is low, the refractive index in ITO layer remains uniform to be ∼0.4 due to the negligible nonlinear effect, i.e. linear case (figure 4(b)). As the incident intensity increases to 1 GW cm^{-2}, the refractive index in ITO increases spatially due to the localized resonant mode, which holds a similar distribution to the electric field (figures 4(c) and (d)). Simultaneously, E_x component gradually contributes to the refractive index change. The field distribution and refractive index iteratively affect each other and both consequently present an asymmetric distribution along both x- and y-axes (figures 4(c)–(h)). The phase and amplitude of E_x component decrease even more in comparison with the counterparts of E_x component. Therefore, the polarization switching is mainly attributed to the resonance along y-axis. As the incident power increases further, the refractive index gets much larger but holds the similar trend, which is even three-fold higher than the counterpart in linear case along the y-axis (figure 4(h)). Such evolution of field and refractive generates the different variation trends of E_x and E_y components, and thus supports the all-optical polarization tuning.

The performance polarization tuning is dependent not only on the phase difference between two orthogonal electric field components, but also on their amplitude ratio. As a proof of concept, a linearly polarized light with polarization angle 0.61π is intentionally selected to provide an amplitude ratio of 1. When the incident intensity is 0.01 GW cm^{-2}, two electric fields still have a π phase difference after reflection (figures 2(b) and 3). Naturally, the reflected light maintains the linear polarization state being the same to the incident counterpart (figure 5). As the intensity increases to 1 GW cm^{-2}, the phase difference is 0.76π and the amplitude ratio is 0.78. Thus, an elliptical polarization state is generated with a polarization axis along 128° with respect to x-axis. As the intensity gradually increases to 3.5 GW cm^{-2}, the E_y component oscillates in advance of 0.5π in comparison with E_x component. Simultaneously, their amplitudes are almost equal. Therefore, the

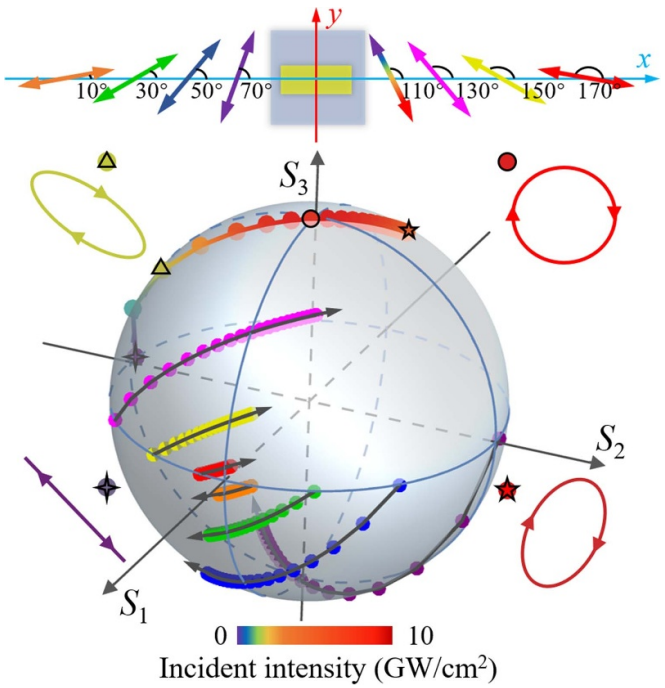

Figure 5. Dependence of the polarization state of the reflected light on the polarization angle and intensity of incident light represented in the Poincaré sphere. Black arrows indicate the intensity increasing direction. Here, $L = 325$ nm and $W = 235$ nm. Four insets represent the polarization ellipses of reflected light under the illumination of different intensity. Upper panel shows the polarization direction of the incident light and the corresponding polarization trajectories are plotted in Poincaré sphere with the same color.

polarization of the reflected light is switched from elliptical to right circular polarization state. The polarization state grows to be elliptical again under the illumination of higher intensity (four polarization ellipses in figure 5). The evolution of polarization is also plotted as indicated by the gradient color in Poincaré sphere (figure 5).

The phase difference between two electric field is fixed when the structure is designed, while the amplitude ratio can be controlled via the polarization state of the incident light. Therefore, it is promising to generate more polarization states by rotating the incident polarization state. The Poincaré sphere is employed to characterize the capability of polarization generation of the proposed metasurface The Stokes parameters are defined as $S_0 = E_x^2 + E_y^2$, $S_1 = E_x^2 - E_y^2$, $S_2 = 2E_xE_y\cos\delta$ and $S_3 = 2E_xE_y\sin\delta$. The dependence of the polarization state of reflected light on the incident polarization angle is explored as the incident power increases (figure 5). By fixing the structure size, the structure is illuminated by a linearly polarized light with different polarization angles (10°, 30°, 50°, 70°, 110°, 130°, 150° and 170°). The intensity-dependent polarization trajectories of each reflected light are plotted in different colors on the same Poincaré sphere (figure 5). Significantly, when the polarization angle of the incident light is less than 90°, the polarization trajectory is mainly spread over the area $S_3 < 0$ and $S_2 > 0$. In contrast, when the polarization angle is larger than 90°, the polarization trajectories are mainly spread in the area of $S_3 > 0$ and $S_2 < 0$. The total polarization state trajectories are spread over almost half of the Poincaré sphere, which promises a prospect polarization tuning capability with single metasurface.

To conclude, all-optical polarization tuning is proposed at NIR range using a nonlinear metasurface. Based on the strong nonlinear refractive index effect of ENZ material, a large refractive index change is spatially induced to support a synthetic control of phase difference and amplitude ratio of two orthogonal electric fields by altering the incident light intensity. Significantly, a phase difference is tuned in a range greater than 0.61π. As a result, the polarization state of reflected light is dynamically and continuously tuned from a linear polarization to an elliptical polarization, and then to a circular polarization. Moreover, more polarization states can be obtained with the same metasurface by changing the polarization angle of the incident light covering about half of the Poincaré sphere. We believe that the proposed all-optical approach can be extended to more photonic functionalities active control and facilitate their practical applications.

Data availability statement

All data that support the findings of this study are included within the article (and any supplementary files).

Funding

The authors acknowledge financial support by National Key R&D Program of China (2022YFB4601701); Shaanxi Key Science and Technology Innovation Team Project (2021TD-56); Young Talent Recruiting Plans of Xi'an Jiaotong University.

ORCID iDs

Weitao Jiang https://orcid.org/0000-0002-9222-2844
Yanpeng Zhang https://orcid.org/0000-0002-0954-7681
Lei Zhang https://orcid.org/0000-0002-5113-1786

References

[1] Rubin N A, Shi Z and Capasso F 2021 *Adv. Opt. Photon.* **13** 836–970
[2] Yue Z *et al* 2022 *Opto-Electron. Sci.* **1** 210014
[3] Zheng C, Li J, Liu J, Li J, Yue Z, Li H, Yang F, Zhang Y, Zhang Y and Yao J 2022 *Laser Photon. Rev.* **16** 2200236
[4] Earl S K, James T D, Gómez D E, Marvel R E, Haglund R F and Roberts A 2017 *APL Photonics* **2** 016103
[5] Wu P C, Sokhoyan R, Shirmanesh G K, Cheng W H and Atwater H A 2021 *Adv. Opt. Mater.* **9** 2100230
[6] Meng C, Thrane P C V, Ding F and Bozhevolnyi S I 2022 *Nat. Commun.* **13** 1–7
[7] Yang Y, Kelley K, Sachet E, Campione S, Luk T S, Maria J-P, Sinclair M B and Brener I 2017 *Nat. Photon.* **11** 390–5
[8] Wang K, Seidel M, Nagarajan K, Chervy T, Genet C and Ebbesen T 2021 *Nat. Commun.* **12** 1–9
[9] Jaffray W *et al* 2022 *Nat. Commun.* **13** 3536
[10] Niu X, Hu X, Xu Y, Yang H and Gong Q 2021 *Adv. Photon. Res.* **2** 2000167

[11] Wang K, Li M, Hsiao H-H, Zhang F, Seidel M, Liu A-Y, Chen J, Devaux E, Genet C and Ebbesen T 2021 *ACS Photon.* **8** 2791–9
[12] Boyd R W 2020 *Nonlinear Optics* (New York: Academic Press)
[13] Kinsey N, DeVault C, Boltasseva A and Shalaev V M 2019 *Nat. Rev. Mater.* **4** 742–60
[14] Reshef O, De Leon I, Alam M Z and Boyd R W 2019 *Nat. Rev. Mater.* **4** 535–51
[15] Jaffray W, Saha S, Shalaev V M, Boltasseva A and Ferrera M 2022 *Adv. Opt. Photon.* **14** 148–208
[16] Capretti A, Wang Y, Engheta N and Dal Negro L 2015 *ACS Photonics* **2** 1584–91
[17] Alam M Z, De Leon I and Boyd R W 2016 *Science* **352** 795–7
[18] Hao J, Wang J, Liu X, Padilla W J, Zhou L and Qiu M 2010 *Appl. Phys. Lett.* **96** 251104
[19] Shrestha S, Wang Y, Overvig A C, Lu M, Stein A, Negro L D and Yu N 2018 *ACS Photonics* **5** 3526–33
[20] Sun S *et al* 2012 *Nano Lett.* **12** 6223–9
[21] Zheng G, Muhlenbernd H, Kenney M, Li G, Zentgraf T and Zhang S 2015 *Nat. Nanotechnol.* **10** 308–12
[22] Heiden J T, Ding F, Linnet J, Yang Y, Beermann J and Bozhevolnyi S I 2019 *Adv. Opt. Mater.* **7** 1801414
[23] Reshef O, Giese E, Zahirul Alam M, De Leon I, Upham J and Boyd R W 2017 *Opt. Lett.* **42** 3225–8
[24] Alam M Z, Schulz S A, Upham J, De Leon I and Boyd R W 2018 *Nat. Photon.* **12** 79–83
[25] Cheng L, Alaee R, Safari A, Karimi M, Zhang L and Boyd R W 2021 *ACS Photon.* **8** 585–91
[26] Johnson P B and Christy R W 1972 *Phys. Rev.* B **6** 4370–9
[27] Campione S, Brener I and Marquier F 2015 *Phys. Rev.* B **91** 121408
[28] Ma W, Liu Z, Kudyshev Z A, Boltasseva A, Cai W and Liu Y 2021 *Nat. Photon.* **15** 77–90
[29] Wiecha P R and Muskens O L 2020 *Nano Lett.* **20** 329–38